Electronic Supplementary Material (ESI) for Journal of Materials Chemistry B.

Supporting Information

Bright luminescent optically engineered core/alloyed shell quantum dots: An ultrasensitive signal transducer for dengue virus RNA via localized surface plasmon resonance-induced hairpin hybridization†

Oluwasesan Adegoke,[a] Enoch Y. Park[*,a,b]

[a] *Laboratory of Biotechnology, Research Institute of Green Science and Technology, Shizuoka University, 836 Ohya, Suruga-ku, Shizuoka 422-8529, Japan.*
E-mail: adegoke.sesan@mailbox.co.za , park.enoch@shizuoka.ac.jp

[b] *Laboratory of Biotechnology, Department of Bioscience, Graduate School of Science and Technology, Shizuoka University, 836 Ohya, Suruga-ku, Shizuoka 422-8529, Japan*

† Electronic supplementary information (ESI) available: MTT viability assay of Qdot606 to HEK 293T cells, PL lifetime decay curves of the Qdots, TEM images of the Qdot-AuNPs-MB biosensor conjugates, DLS and zeta potential of the Qdot-AuNP nanohybrids, DLS and zeta potential curves for the Qdot-AuNP-MB biosensor conjugate, fluorescence quenching effects of $_{L}$-cysteine AuNPs on the Qdots after conjugation and the fluorescence quenching effects of the MB on the Qdot-AuNP conjugates, fluorescence quenching effects of $_{L}$-cysteine AuNPs on the Qdots after conjugation and the fluorescence quenching effects of the MB on the Qdot-AuNP conjugates.

[*] Laboratory of Biotechnology, Research Institute of Green Science and Technology, Shizuoka University, 836 Ohya, Suruga-ku, Shizuoka 422-8529, Japan. E-mail: park.enoch@shizuoka.ac.jp

Cell viability assay

A cell viability experiment was carried out on the newly developed GSH-CdSe/ZnSeS core/alloyed shell Qdots using the methyl thiazol tetrazolium bromide (MTT) assay.[1] To each well of a 96-well plate, 100 µL cell suspension containing HEK 293T cells was seeded, resulting in a final density of 2 x 10^5 cells/mL. After incubation of the cells for 48 hr at 37°C, different concentrations of Qdot606 (used as a representative Qdot), from 0.01–0.1 mg/mL, were added to the wells. HEK 293T cells with no dots were used as the control. A 10 µL solution of MTT reagent (25 mg in 5 mL of PBS) was added to the cells containing Qdots after incubation for 24 hr. Afterward, the cells were incubated for an additional 4 hr, and 200 µL of PBS was added to each well. After removal of the media, 200 µL of DMSO was used to dissolve the formazan blue formed in the cell. A microplate reader was used to measure the absorbance of the cell assay at 530 nm. Triplicate measurements were carried out, and the average value was used.

Cell viability result

The toxicity of Qdots is a major concern for their widespread applications in biological systems. The coating of non-toxic shell layers is a strategic way to protect the Cd ion from leakage into the cell to render the Qdot non-toxic or with reduced toxicity. The cytotoxicity level of Cd-based chalcogenide Qdots is still debatable within the scientific community with varying theories of potential route for cell death.[2] In this work, we have carried out a simple MTT viability assay to probe the cytotoxicity of the newly synthesized GSH-CdSe/ZnSeS Qdots. Qdot606 was chosen as the representative Qdots for this analysis. The dose dependent (0.01 – 0.1 mg/mL) cell viability of Qdot606 to HEK 293T cells after 48 hr of exposure is shown in Fig. S-1. We found no apparent toxicity of the Qdots to the cells as the cell viability results show that no cell death occur. It is imperative to emphasize that the mg/mL dose level of Qdots used in this work is much higher than the µg/mL dose level usually reported in the

literature.[3-5] We can emphatically draw the conclusion that GSH-CdSe/ZnSeS Qdots exhibit excellent cell viability to HEK 293T cells.

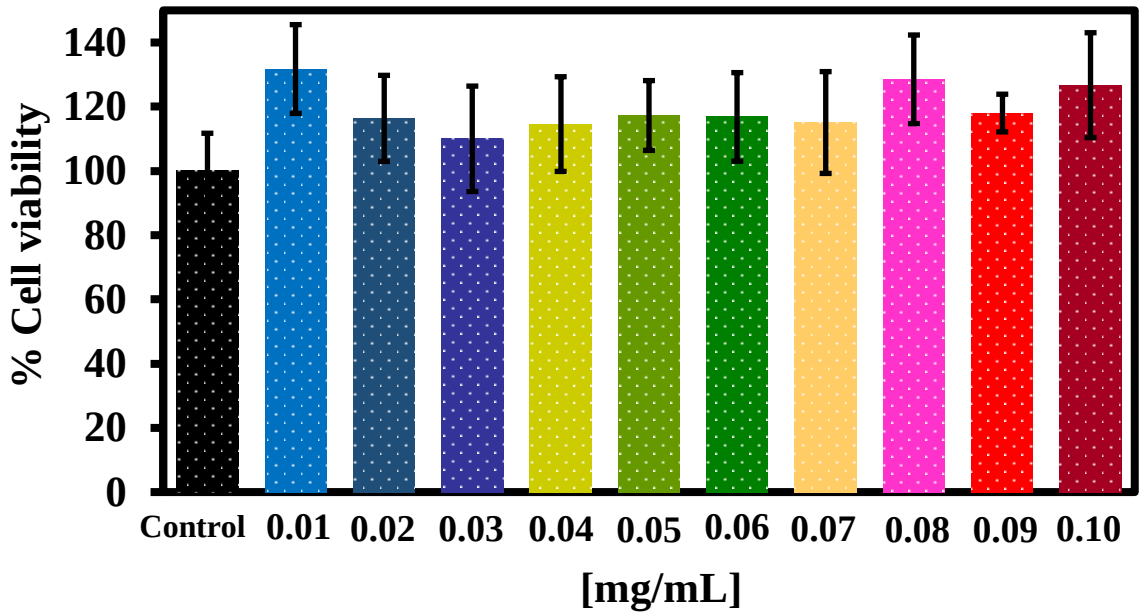

Fig. S-1. MTT viability assay of Qdot606 to HEK 293T cells.

PL Lifetime

Supplementary Fig. S-2 shows the single monoexponential PL decay curves for the size-dependent Qdots, and the PL lifetime value for each Qdot is indicated on each figure. Judging from the lifetime values, we can generally infer that no direct relationship exists between the Qdot size increase and PL QY for Qdot 614, Qdot618 or Qdot622. We believe that the single-dot monoexponential characteristic of the PL lifetime is induced by fluctuations that are directly aligned with single-dot emission intensities. These fluctuations in the radiative rate were not apparent for Qdot582, Qdot694 and Qdot606 because an increase in the particle size and PL QY was effectively correlated with an increase in the PL lifetime. If fluctuation in the radiative rate exists, a decline in the lifetime should correspond to an increase in the PL QY.[6] However, this was not the case, judging from the PL lifetime of Qdot614, Qdot618 and Qdot622. Surface defect states influenced by external trap sites generally lead to non-

radiative exciton relaxation pathways in single ensemble Qdots.[7] Therefore, the PL lifetime fluctuation reflects the coupling of the excited state of the Qdots to non-radiative exciton trap states.

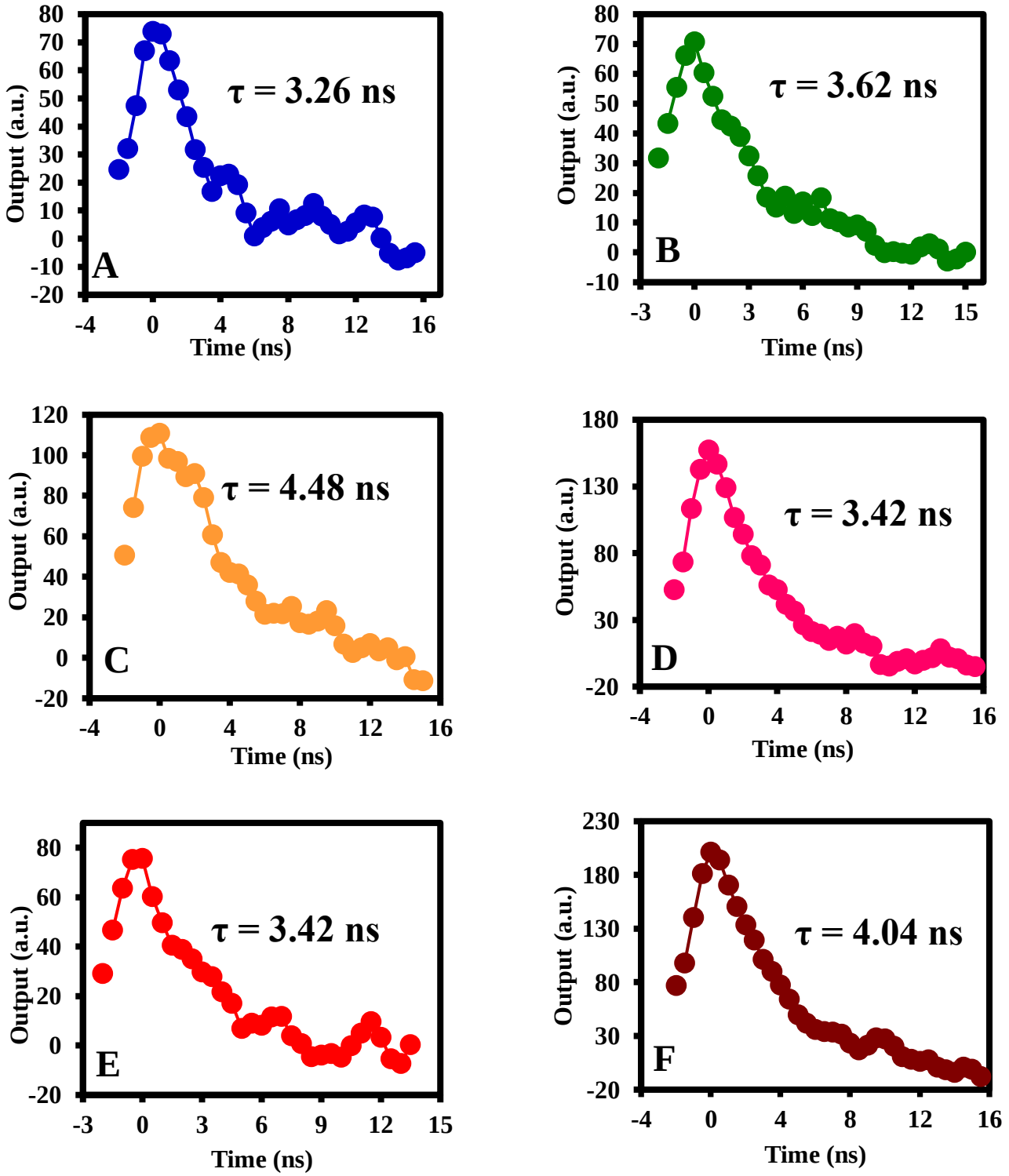

Fig. S-2. PL lifetime decay curves of (A) Qdot582, (B) Qdot594, (C) Qdot606, (D) Qdot614, (E) Qdot618 and (F) Qdot622.

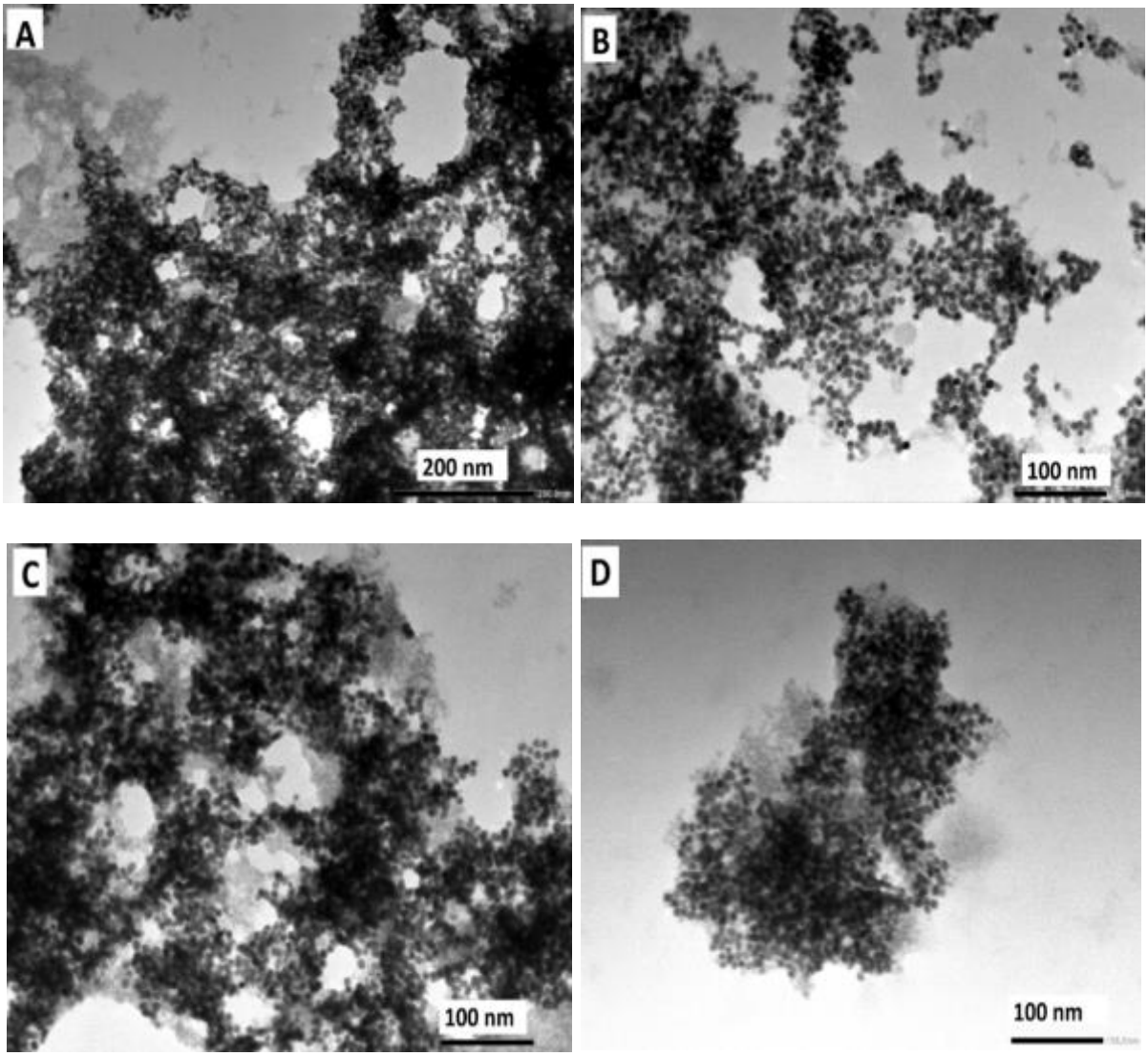

Fig. S-3. TEM images of (A) Qdot582-AuNPs-MB, (B) Qdot594-AuNPs-MB, (C) Qdot606-AuNPs-MB and (D) Qdot618-AuNPs-MB.

DLS and ZP of Qdot-AuNP conjugates

Fig. S-4A-D shows the DLS curves of the Qdot582-AuNP, Qdot594-AuNP, Qdot606-AuNP and Qdot618-AuNP conjugates. In this section, we utilize DLS as a technique to probe the aggregation state and dispersity of the conjugates. It is expected that the hydrodynamic size of the Qdot-AuNP conjugates should be higher than the size obtained for the individual Qdots and AuNPs. The values obtained are 87.7±21.6 nm for Qdot582-AuNPs, 57.5±21.0 nm for Qdot594-AuNPs, 69.1±38.8 nm for Qdot606-AuNPs and 52.3±21.5 nm for Qdot618-AuNPs. The values obtained indicate that the hydrodynamic particle size of the conjugates are still within the range of colloidal monodispersity. Although, the particles are more broadly distributed. This is expected due to the variability in the size distribution of the Qdots and AuNPs. The TEM images shown in Fig. 5 also confirms the monodispersity of the conjugates. Since the hydrodynamic size value of the conjugates are less than 100 nm, we can conclude that the conjugate solution are unagglomerated.

The corresponding ZP of the conjugates are shown in Fig. S-4A1-D1. ZP analysis was used to probe the colloidal stability of the conjugates. The values obtained are -40.9±4.2 mV for Qdot582-AuNPs, -41.2±4.4 mV for Qdot594-AuNPs, -39.0±4.3 mV for Qdot606-AuNPs and -42.5±5.0 mV for Qdot618-AuNPs. The ZP curves of the conjugates displayed high degree of stability as evident from the lack of peak splitting. The ZP values confirms that the colloidal solution of the conjugates are within the range of high colloidal stability. This imply that the strong binding of the Qdots to AuNPs did not distort the stability of the conjugate system, hence making them suitable for further conjugation to the MBs. Retaining the stability of nanoparticles within a conjugates system is challenging due to factors such as steric hindrance, aggregation and surface defects. Maintaining the stability of the conjugate system provides evidence that both the Qdots and AuNPs exhibit good optical properties.

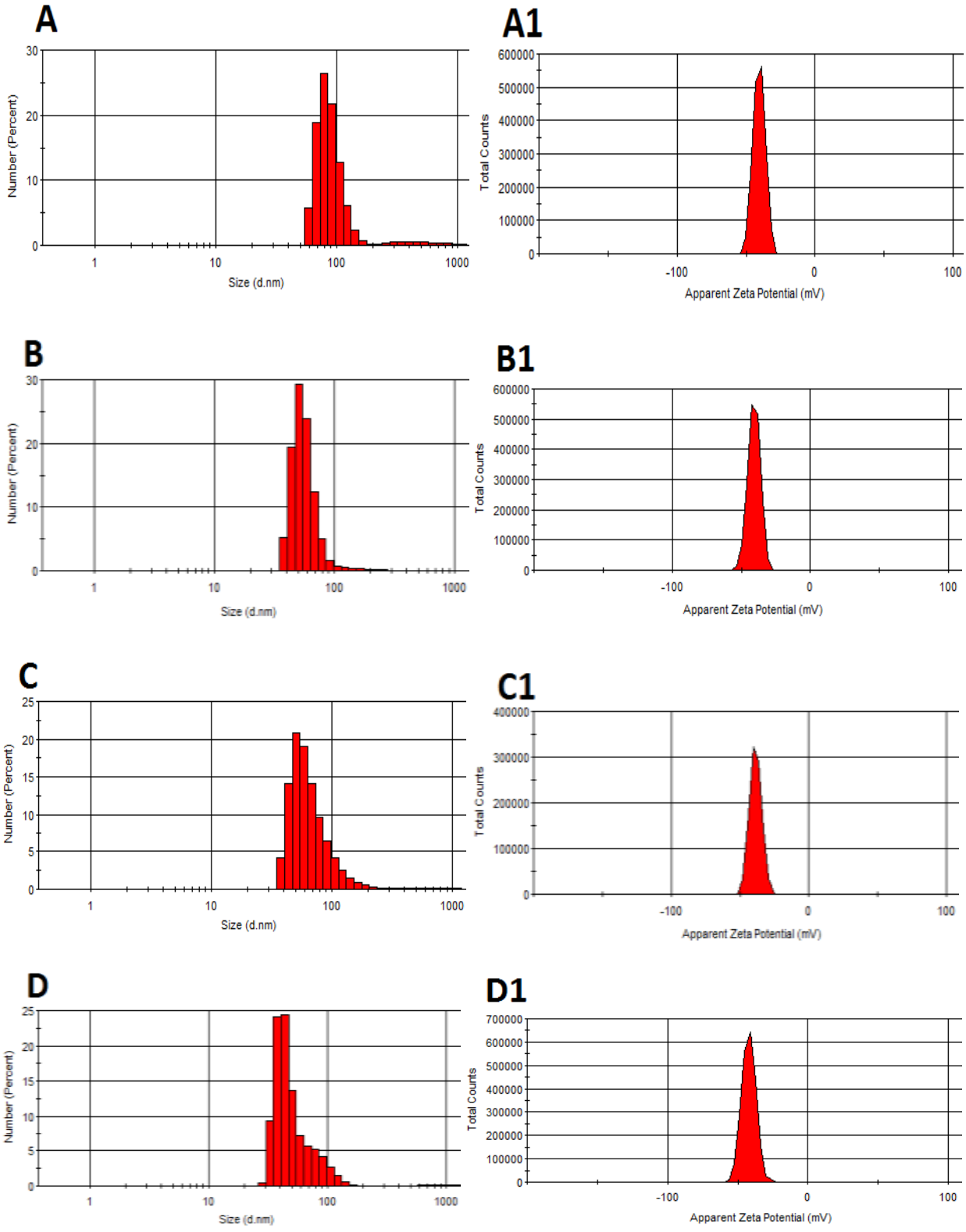

Fig. S-4. DLS (A-D) and zeta potential (A1-D1) curves for Qdot582-AuNP (A, A1), Qdot594-AuNP (B, B1), Qdot606-AuNP (C, C1) and Qdot618-AuNP (D, D1).

DLS and ZP of Qdot-AuNP-MB conjugates

The DLS plots of the Qdot-AuNP-MB conjugates are shown in Fig. S-5A-D. The ratio of Qdot-AuNPs to the MB was (2:0.5 v/v). As we have probed the monodispersity and aggregation state of the Qdot-AuNP conjugates in the previous section, we hereby perform similar assessment for the Qdot-AuNP-MB conjugates. The DLS values obtained are 126.9±23.2 nm for Qdot582-AuNP-MB, 74.4±27.2 nm for Qdot594-AuNP-MB, 102.4±22.4 nm for Qdot606-AuNP-MB and 96.9±19.8 nm for Qdot618-AuNP-MB. We directly observed an increase in the hydrodynamic particle size in comparison to the Qdot-AuNP conjugates. The increase is due to the strong binding of the Qdot-AuNP conjugates to the MB. With the exception of Qdot594-AuNP-MB and Qdot618-AuNP-MB, the hydrodynamic particle size of Qdot582-AuNP-MB and Qdot606-AuNP-MB are greater than 100 nm. This values obtained are not surprising but expected due to the coarseness in the particle distribution following the strong binding to the MB.

Fig. S-5A1-D1 shows the corresponding ZP plots for the Qdot-AuNP-MB conjugates. The emphasis here is to probe the colloidal stability of the resulting Qdot-AuNP-MB conjugates as we have performed above for the Qdot-AuNP conjugates. The values obtained are -34.8±3.6 mV for Qdot582-AuNPs-MB, -36.6±7.5 mV for Qdot594-AuNPs-MB, -35.6±4.1 mV for Qdot606-AuNPs-MB and -36.6±5.5 mV for Qdot618-AuNPs-MB. It is quite surprising that after the strong binding of the plasmonic fluorophore to the MB, the ZP of the resulting conjugates are still within the range of high colloidal stability. We attribute the strong stability of the conjugates to the spectacular optical properties of the Qdots and AuNPs.

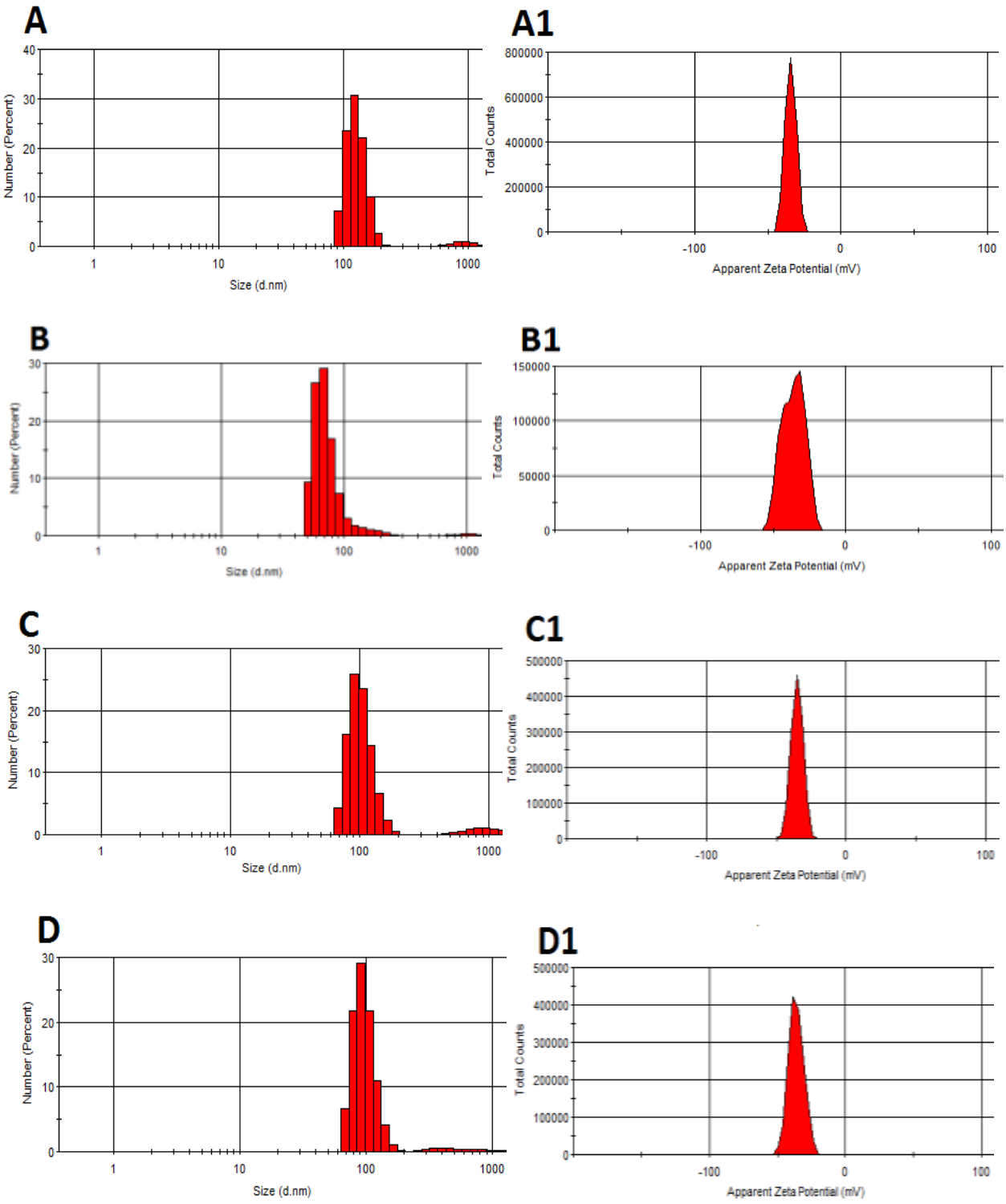

Fig. S-5. DLS (A-D) and zeta potential (A1-D1) curves for Qdot582-AuNP-MB (A, A1), Qdot594-AuNP-MB (B, B1), Qdot606-AuNP-MB (C, C1) and Qdot618-AuNP-MB (D, D1) biosensor conjugate probes.

PL Quenching effects after conjugation

Fig. S6A-D shows the fluorescence quenching effect of Qdot-AuNP and Qdot-AuNP-MB conjugates. After conjugation of AuNPs to the Qdots, the strong binding effect which could arise from energy transfer from the Qdots to AuNP induces the fluorescence of the Qdots to be quenched. The quenching effects of the MBs on the fluorescence of the Qdot-AuNP conjugate are also shown.

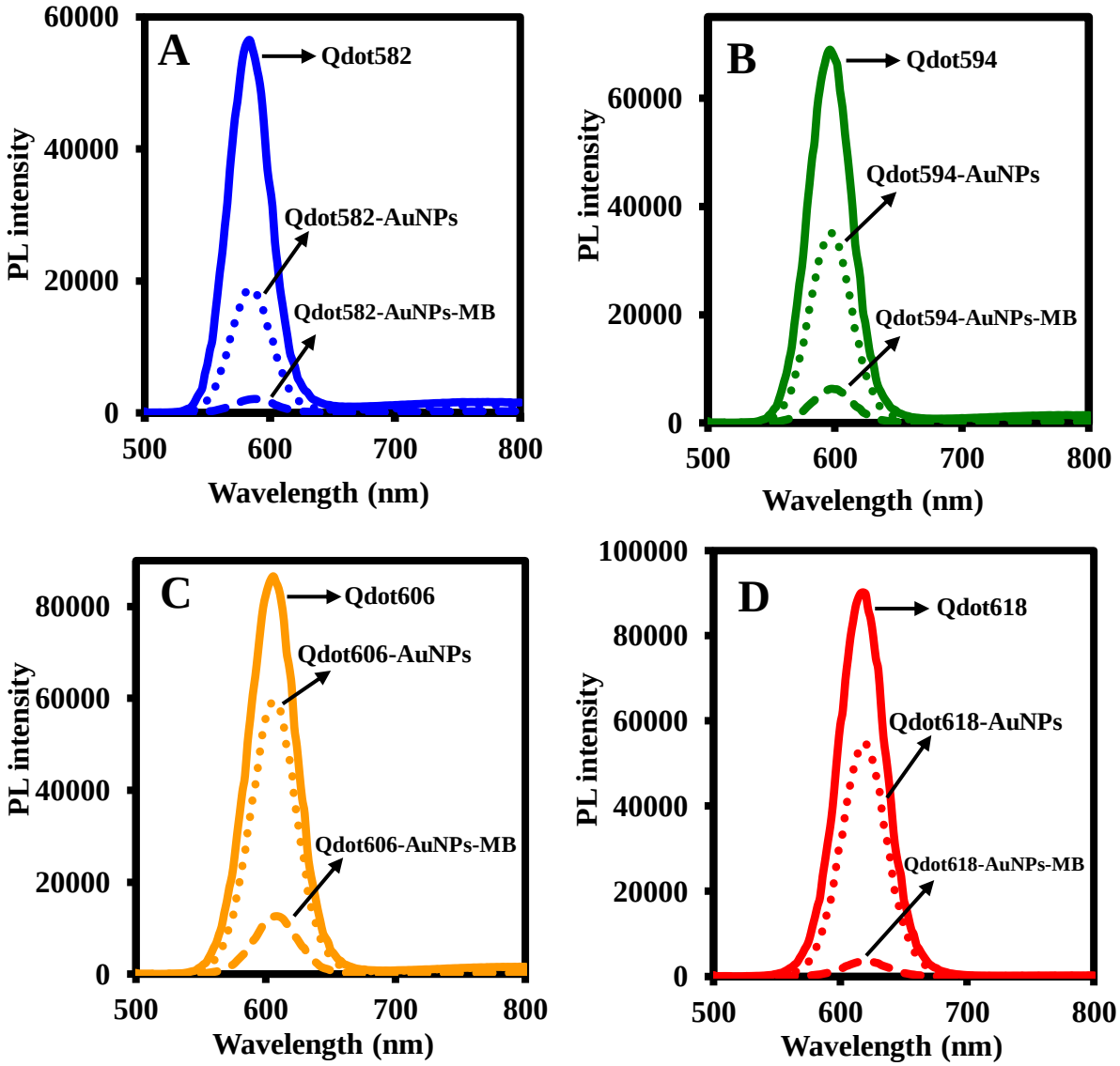

Fig. S-6. Fluorescence quenching effects of L-cysteine AuNPs on the Qdots after conjugation and the fluorescence quenching effects of the MB on the Qdot-AuNP conjugates.

In this section, we discuss the comparison in detection sensitivity of the Qdot-AuNP-MB biosensor probe with the Qdot-MB probe (having no influence of LSPR signal from AuNPs). The highest concentration of DENV detected by the Qdot-AuNP-MB biosensor probe was used for comparison. Fig. S-7A-D shows the comparison in PL intensity of the Qdot-AuNP-MB and Qdot-MB probes before and after detection of the target DENV. Our analysis shows that LSPR signal from AuNPs enhanced the sensitivity of the biosensor probe, hence making the Qdot-AuNP-MB a more superior biosensor probe.

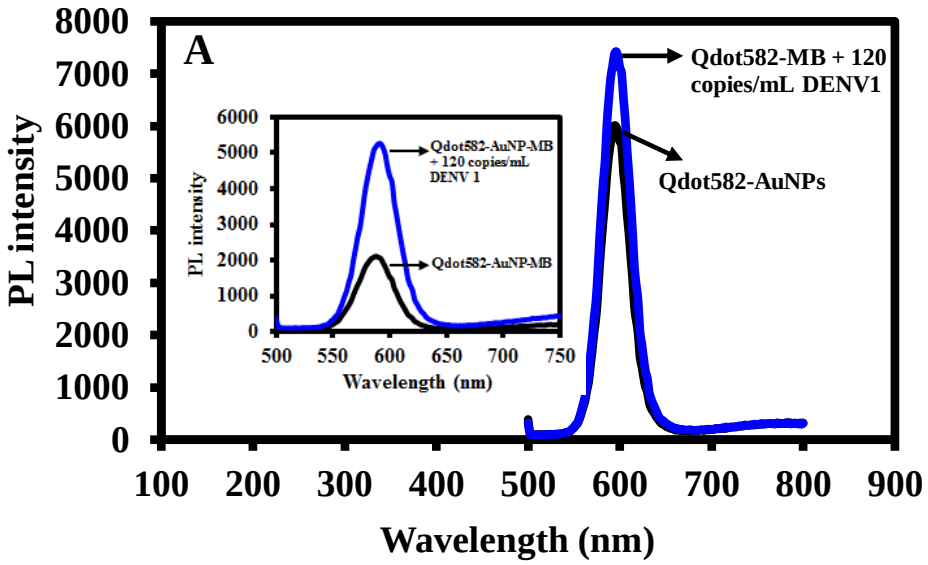

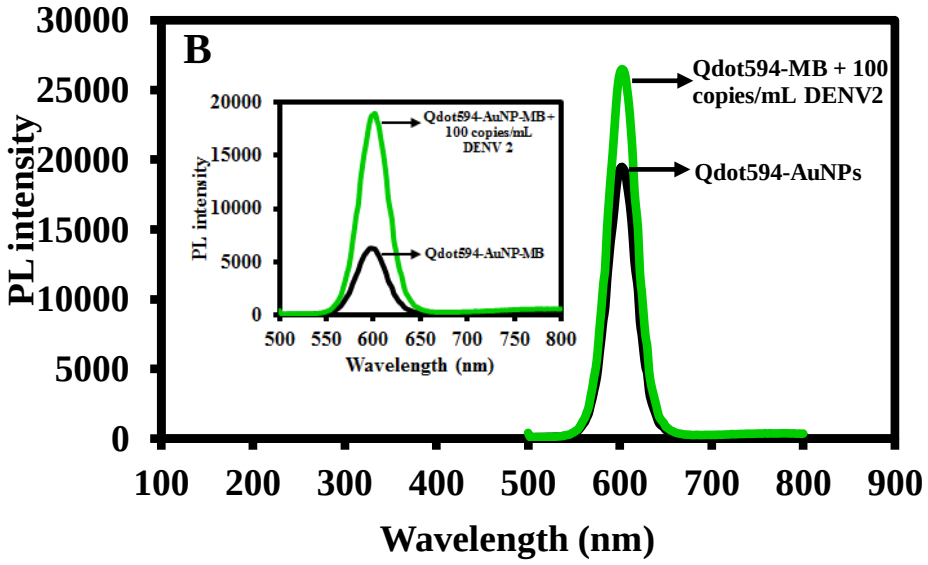

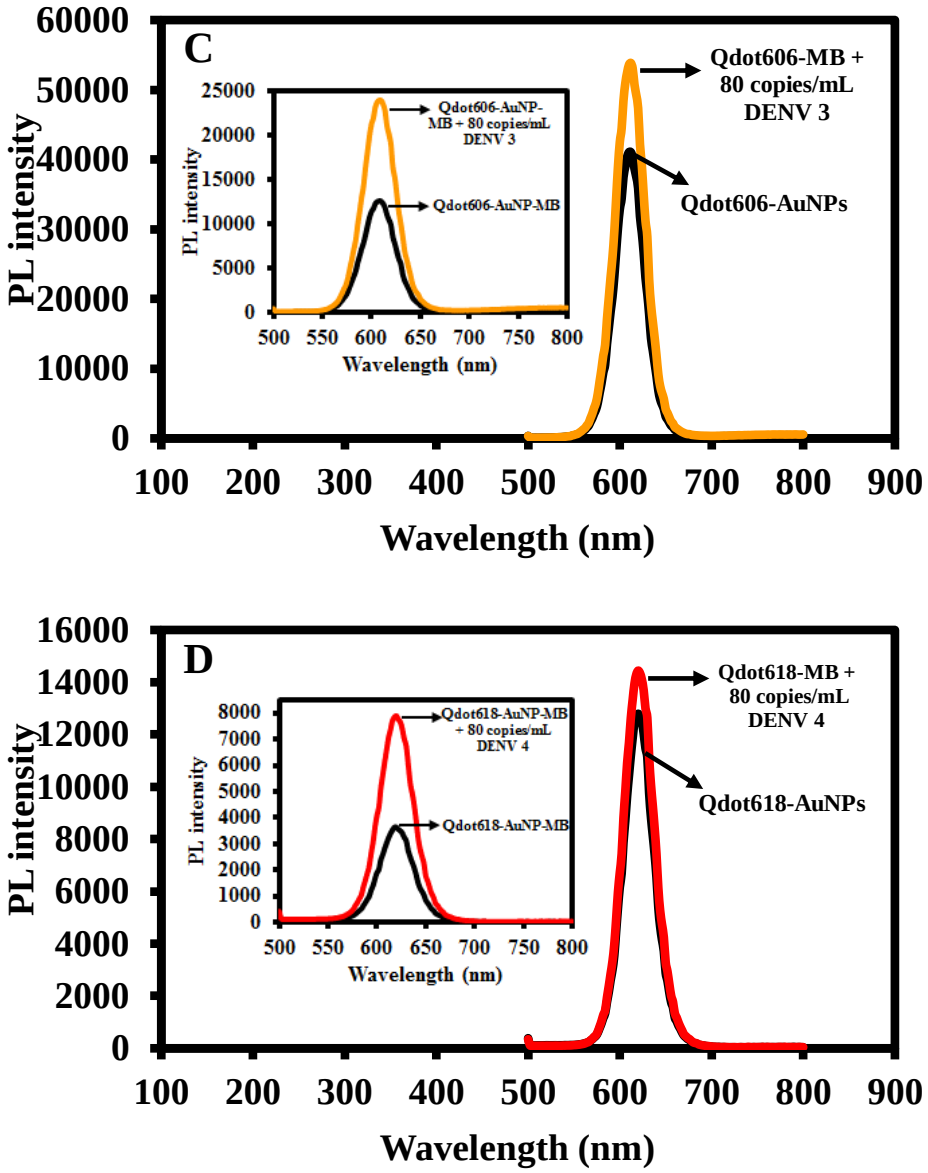

Fig. S-7. Comparison of the PL switch on detection of DENV1-4 using the Qdots-MB probe and the Qdot-AuNP-MB biosensor probe (inset). Detection of (A) 120 copies/mL DENV1, (B) 120 copies/mL DENV2, (C) 80 copies/mL DENV3 and (D) 80 copies/mL DENV4.

References

1. T. Mosmann, *J. Immunol. Methods*, 1983, **65**, 55–63.
2. R. A. Hardman, *Environ. Health Perspect.*, 2006, **114**, 165–172.
3. J. Liu, R. Hu, J. Liu, B. Zhang, Y. Wang, X. Liu, W. C. Law, L. Liu, L. Ye, K. T. Yong, *Mat. Sci. Eng. C-Mater.*, 2015, **57**, 222–231.
4. M. S. Stan, I. Memet, C, Sima, T. Popescu, V. S. Teodorescu, A. Hermenean, A. *Chem. Biol. Interact.*, 2014, **220**, 102–115.
5. M. Yan, Y. Zhang, H. Qin, K. Liu, M. Guo, Y. Ge, M. Xu, Y. Sun, X. Zheng, *Int. J. Nanomed.*, 2016, **11**, 529–542.
6. M. G. Bawendi, P. J. Carroll, W. L. Wilson, L. E. Brus, *J. Chem. Phys.*, 1992, **96**, 946–954.
7. O. Adegoke, M.-W. Seo, T. Kato, S. Kawahito, E. Y. Park, J. Mater. Chem B, 2016, **4**, 1489–1498.